# Conformation-Dependent Swinging of the Matrix Loop m2 of the Mitochondrial *Saccharomyces cerevisiae* ADP/ATP Carrier†

Cécile Dahout-Gonzalez,[#] Claire Ramus,[‡] Emmanuel Philippe Dassa,[#] Anne-Christine Dianoux,[#] and Gérard Brandolin*,[#]

*Laboratoire de Biochimie et Biophysique des Systèmes Intégrés, UMR 5092 CNRS-CEA-Université Joseph Fourier, Département de Réponse et Dynamique Cellulaires, CEA-Grenoble, 17 avenue des Martyrs, 38054 Grenoble Cedex 9, France, and Laboratoire de Chimie des Protéines, ERM-0201 INSERM-CEA, Département de Réponse et Dynamique Cellulaires, CEA-Grenoble, 17 avenue des Martyrs, 38054 Grenoble Cedex 9, France*

*Received July 27, 2005; Revised Manuscript Received September 30, 2005*

ABSTRACT: Structure−function relationships of the membrane-embedded *Saccharomyces cerevisiae* mitochondrial ADP/ATP carrier were investigated through two independent approaches, namely, limited proteolysis and cysteine labeling. Experiments were carried out in the presence of either carboxyatractyloside (CATR) or bongkrekic acid (BA), two specific inhibitors of the ADP/ATP transport that bind to two distinct conformers involved in the translocation process. The proteolysis approach allowed us to demonstrate (i) that N- and C-terminal extremities of ADP/ATP carrier are facing the intermembrane space and (ii) that the central region of the carrier corresponding to the matrix loop m2 is accessible to externally added trypsin in a conformation-sensitive manner, being cleaved at the Lys163-Gly164 and Lys178-Thr179 bonds in the carrier-CATR and the carrier-BA complexes, respectively. The cysteine labeling approach was carried out on the S161C mutant of the ADP/ATP carrier. This variant of the carrier is fully active, displaying nucleotide transport kinetic parameters and inhibitor binding properties similar to that of wild-type carrier. Alkylation experiments, carried out on mitochondria with the nonpermeable reagents eosin-5-maleimide and iodoacetamidyl-3,6-dioxaoctanediamine-biotin, showed that Cys 161 is accessible from the outside in the carrier-CATR complex, whereas it is masked in the carrier-BA complex. Taken together, our results indicate that the matrix loop m2 connecting the transmembrane helices H3 to H4 intrudes to some extent into the inner mitochondrial membrane. Its participation in the translocation of ADP/ATP is strongly suggested, based on the finding that its accessibility to reagents added outside mitochondria is modified according to the conformational state of the carrier.

The adenine nucleotide carrier (Anc)[1] is a nuclear-encoded protein located in the mitochondrial inner membrane. Under physiological conditions, it catalyzes the one-to-one exchange of ATP, generated inside mitochondria by oxidative phosphorylation, against cytoplasmic ADP. The mitochondrial ADP/ATP exchange process can be blocked by two very specific inhibitors, namely, carboxyatractyloside (CATR) on one hand and bongkrekic acid (BA) on the other. CATR and BA bind with high affinity to two distinct preexisting conformations of the carrier referred to as CATR and BA conformations, respectively, resulting in the formation of stable CATR- and BA-carrier complexes. It has been proposed that the transition between the CATR and BA conformations is involved in ADP/ATP transport (for review, see refs *1* and *2*). Therefore, characterization of the carrier conformations that are locked by either CATR or BA would shed light on molecular events occurring during the transport process.

The ADP/ATP carrier belongs to a wide family of membrane proteins that carry out the exchange of various metabolites across the mitochondrial inner membrane (*3*). Members of this family share common features, i.e., similar molecular weight of about 30 kDa, a so-called tripartite organization consisting of three sequence repeats of about 100 amino acid residues each, and the presence in each repeat of the conserved signature motif P-X-[D/E]-X-X-[K/R] (*3*). The only mitochondrial carrier for which high resolution structural data have been obtained so far is the bovine ADP/ATP carrier, which we have recently crystallized as the CATR-carrier complex (*4*). The 2.2 Å resolution model of the CATR conformation of the bovine carrier depicts a

† Support for this work was provided by the Commissariat à l'Energie Atomique, the Centre National de la Recherche Scientifique, the Région Rhône-Alpes, and the University Joseph Fourier of Grenoble. E.P.D. was supported by a fellowship from the Région Rhône-Alpes.

* Address correspondence to Gérard Brandolin, BBSI/DRDC, CEA-Grenoble, 17 avenue des Martyrs, 38054 Grenoble Cedex 9 France. Phone: 33(0)438789233. Fax: 33(0)438785185. E-mail: gbrandolin@cea.fr.

[#] Laboratoire de Biochimie et Biophysique des Systèmes Intégrés, UMR 5092 CNRS-CEA-Université Joseph Fourier.

[‡] Laboratoire de Chimie des Protéines, ERM-0201 INSERM-CEA.

[1] Abbreviations: Anc2($His_6$)p, *S. cerevisiae* adenine nucleotide carrier isoform 2 with a six histidine extension at C-terminal end; ATR, atractyloside; BA, bongkrekic acid; CATR, carboxyatractyloside; DDM, dodecyl maltoside; DDT, dithiothreitol; EM, emulphogen; EMA, eosin-5-maleimide; ESI-MSMS, electrospray ionization-tandem mass spectrometry; HTP, hydroxyapatite; IMAC, immobilized metal-ion affinity chromatography; i-PEO-biotin, iodoacetamidyl-3,6-dioxaoctanediamine-biotin; MALDI-TOF, matrix-assisted laser desorption ionization-time-of-flight; MW, molecular weight; Ni-NTA, nickel-nitrilotriacetic acid; PVDF, polyvinylidene difluorure; SBTI, soybean trypsic inhibitor; SDS, sodium dodecyl sulfate; SPAGE, SDS−polyacrylamide gel electrophoresis; SMP, sub-mitochondrial particles; TM, transmembrane.

10.1021/bi0514820 CCC: $30.25 
Published on Web 11/12/2005

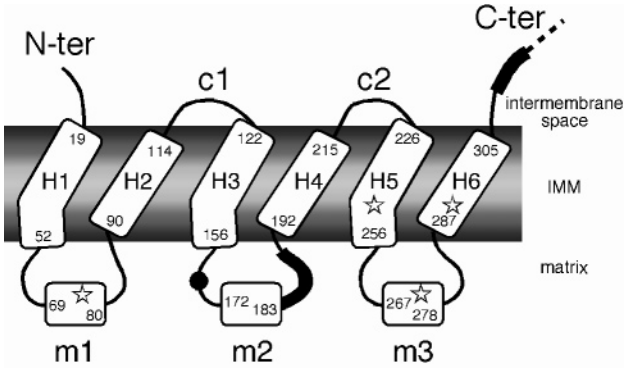


FIGURE 1: Schematic representation of the postulated arrangement of yeast Anc2p in the mitochondrial inner membrane. The model is based on the crystal structure of the bovine ADP/ATP carrier (*5*) and on the sequence alignment of bovine Anc1p and yeast Anc2p performed with ClustalW software. Residues located at extremities of helices are numbered, taking into account the sequence of Anc2p starting at Ser1 (*11*). Boxes represent transmembrane and matrix-exposed helices. Transmembrane helices (H1 to H6) are connected by either cytosolic (c1 and c2) or matrix (m1, m2, and m3) loops. The dashed line at the C-terminal extremity represents the HisTag extension. Heavy black lines indicate the two regions (182−190 and 310−317) labeled by a nontransportable photoactivable ADP derivative (*11*). Endogenous cysteine residue positions (72, 243, 270, and 287) are highlighted with stars, whereas a black circle shows the position of the added cysteine residue in the Anc2-S161C($His_6$)p mutant.

compact transmembrane domain made up of six tilted α-helices, which form a wide cavity opening toward the intermembrane space (*5*). The CATR molecule is located at the bottom of this cavity and strongly interacts with the peptidic chain of the carrier through an intricate network of hydrogen bonds, as well as electrostatic and hydrophobic interactions. Toward the matrix compartment, transmembrane α-helices are connected by three loops (m1, m2, and m3), each containing a 12-residue-long α-helical stretch lying on the membrane surface. The involvement of the matrix loops of the bovine mitochondrial ADP/ATP carrier in the transport mechanism has been suggested by several approaches, including photolabeling studies using photoactivable derivatives of atractyloside or adenine nucleotides (*6*, *7*), site-specific proteolysis (*8*), and chemical labeling of SH groups (*9*, *10*). The role of the central matrix loop of the ADP/ATP carrier in substrate recognition was also demonstrated in the yeast carrier that was photolabeled by 2-azido-3′-*O*-naphthoyl-[$\beta^{32}$P]-ADP at the level of the Ser182−Arg190 region (*11*).

Experiments described in this paper were carried out with a yeast strain expressing the Anc2p isoform of the ADP/ATP carrier carrying a six-histidine extension at its C-terminal end, which has been previously described (*12*). Figure 1 shows a six transmembrane α-helices model of the resulting Anc2($His_6$)p yeast carrier, based on the crystal structure of the bovine carrier and on alignment of the sequences (that share 47% sequence identity) of beef and yeast carriers. Two independent approaches were used in this work to investigate the conformation-sensitive topography of the central matrix loop m2 in CATR- and BA-carrier complexes. The first was based on limited site-specific proteolysis to identify peptide regions accessible to externally added trypsin. In the second approach, we probed the chemical reactivity to membrane-impermeable thiol reagents, of a SH group inserted in the m2 loop of the yeast carrier by site-directed mutagenesis.

The results provide direct experimental evidence that the m2 loop of the yeast Anc2p intrudes into the mitochondrial membrane, and they are discussed in terms of the conformational changes occurring in the peptide chain of the carrier during the nucleotide transport process.

## EXPERIMENTAL PROCEDURES

*Chemicals.* Hydroxyapatite (HTP), poly(vinylidene difluoride) (PVDF) and nitrocellulose 0.2 μm were obtained from Bio-Rad. Emulphogen BC 720 (EM) was purchased from GAF Corporation and purified according to ref *13*. Yeast extract and bactopeptone were from Difco. Lactic acid was from Fluka. Bicinchoninic acid (BCA), carboxyatractyloside (CATR), dodecylmaltoside (DDM), sodium dodecyl sulfate (SDS), bovine serum albumin (BSA), and most other chemicals were obtained from Sigma-Aldrich. Eosin-5-maleimide (EMA) was purchased from Molecular Probes, iodoacetamidyl-3,6-dioxaoctanediamine-biotin (i-PEO-biotin) was from Pierce and $P^1$,$P^5$-Di (adenosine-5′-)-penta-phosphate (Ap5A) was from Calbiochem. Luciferine and luciferase were from Roche. Bongkrekic acid (BA) and $^3$H-atractyloside ([$^3$H]-ATR) were prepared as previously described (*14*, *15*).

*Methods. Strains and Growth Conditions.* The *Saccharomyces cerevisiae* strain used in this study, derived from the W303-1B strain, was JL1-3-1B (*MAT*α, *ade2-1*, *leu2-3*, *112*, *his3-11*, *15*, *trp1-1*, *can1-100*, *ura3-1*, *anc1::LEU2*, *anc2::HIS3*, *anc3::URA3*) *(16). Yeast cells were grown at 28 °C on media made up of 1% (w/v) yeast extract, 2% (w/v) bactopeptone supplemented with 2% (w/v)* D*-glucose (YPD) or with 2% (w/v) lactic acid and 1% (w/v)* $KH_2PO_4$*, final pH 5.5 (YPL).*

*Escherichia coli* XL1-Blue strain (*rec*A1 *end*A1 *gyr*A96 (Nal$^r$) *thi*A1 *hsd*R17 ($r_K^-$ $m_K^+$) *sup*E44 *rel*A1 *lac*$^-$ F′ [Tn10 (tet$^r$) *pro*AB$^+$ *lac*I$^q$ *lac*ZΔ*M*15]) was used to enhance and to subclone the pRS314 phagemid. Bacteria were grown on a standard LB medium supplemented with 0.001% (w/v) ampicillin when necessary.

*Construction of the Mutated ANC2 Gene.* Site-directed mutagenesis of the *ANC2* gene was performed using the standard Quick-change site-directed mutagenesis kit from Stratagene to introduce a cysteine residue at position 161. The pRS314 phagemid containing *ANC2HT*, coding for Anc2($His_6$)p, and its 3′ and 5′ flanking regions (between PstI and SalI restriction sites) was kindly provided by V. Trézéguet (IBGC, Bordeaux). A mutation at position +343 (position +1 corresponding to A from ATG codon) was introduced by Polymerase Chain Reaction (PCR) using the following primers: 5′GCTGACTCCAAGTCCTGTAAAAA-GGGTGGTGC3′ and 5′GCACCACCCTTTTTACAGGACT-TGGAGTCAGC3′ (Genome Express, France) (mutated base is underlined). The mutated *ANC2HT* ORF sequence was checked by DNA sequencing (Genome Express, France), and this fragment was then subcloned into pRS314 vector prior to being used to transform the JL1-3-1B strain, according to the LiCl procedure (*17*). Transformed yeast cells isolated by three repeated inoculations on YPL agar medium were selected for their ability to grow on selective media lacking tryptophan or histidine. Correct integration at the *ANC2* locus

was finally controlled by multiple colony PCR experiments (data not shown).

*Isolation of mitochondria.* Yeast cells grown on YPL were harvested in the late log phase ($OD_{600\ nm}$ between 5 and 6). Mitochondria were prepared following the protocol described in ref *18*. Briefly, spheroplasts obtained after enzymatic digestion of the cell envelope by Zymolyase 20 T (Seikagaku Corp.) were disrupted by Dounce homogeneization in 0.6 M mannitol, 10 mM Tris pH 7.4, 1 mM EDTA, 0.1% (w/v) BSA, and 1 mM PMSF. Mitochondria were isolated by differential centrifugation and washed in the same buffer devoid of BSA and PMSF. Mitochondria were stored in liquid nitrogen. Protein concentration was determined using the BCA reagent kit and BSA as a standard.

[$^3$H]-ATR binding was performed as described previously (*19*). Briefly, mitochondria were suspended at 1 mg of protein/mL in a medium containing 120 mM KCl, 10 mM Tris pH 7.4 and 1 mM EDTA. [$^3$H]-ATR was added at increasing concentrations ranging from 0.1 to 5 $\mu$M. After 45 min of incubation at 0 °C, mitochondria were sedimented and the radioactivity associated with the pellets was measured by scintillation counting. Nonspecific binding was evaluated by a parallel experiment performed in the presence of 20 $\mu$M CATR.

*ADP/ATP Transport Assay in Isolated Mitochondria.* ADP/ATP transport was measured by means of a luminescence assay as described in ref *20*. Freshly prepared mitochondria were incubated at 25 °C in 0.6 M mannitol, 0.1 mM EGTA, 2 mM $MgCl_2$, 10 mM Tris pH 7.4, 10 $\mu$M Ap5A (an inhibitor of adenylate kinase) and 5 $\mu$M α-ketoglutarate (as respiratory substrate) in the presence of 0.1% (w/v) luciferin and 0.1% (w/v) luciferase (*21*). This 2 mL final volume mixture was placed in a spectrophotometry cuvette with continuous stirring, in front of a photomultiplier. It was checked that the amount of luciferin/luciferase added to the medium was not limiting and that the luminescence response was directly proportional to the amount of released ATP. After a 3 min incubation period, ADP (0.1−50 $\mu$M final concentration) was added to initiate the ATP efflux and the related light emission was recorded. The time-course of ATP efflux was monitored over a 5 min period. It was shown in control experiments carried out in the presence of 20 $\mu$M CATR that the ADP/ATP exchange was totally inhibited, thus demonstrating it was strictly mediated by the ADP/ATP carrier. Quantification of released ATP was performed on the basis of the signal amplitude corresponding to additions of 0.5 nmol of ATP as a standard. $K_M$ values for external ADP were determined from initial transport rates, taking into account the concentrations of free ADP (*22*).

*Proteolysis of the Membrane-Bound ADP/ATP Carrier.* Freshly isolated mitochondria expressing Anc2($His_6$)p were first incubated for 10 min at 0 °C at a concentration of 4 mg of total mitochondrial proteins per mL in the presence of either CATR (20 $\mu$M) or BA (20 $\mu$M) in a medium made up of 0.6 M mannitol and 1 mM EDTA, supplemented with 10 mM Tris-HCl, final pH 7.3 or with 10 mM MES, final pH 6.6, respectively. The pH of both suspensions was then adjusted to 8.0 by addition of $NH_4HCO_3$ (0.1 M final concentration) and trypsin was added at a final protease-to-mitochondrial proteins ratio of 1/200 to 1/50 (w/w). Proteolytic digestion was carried out at 4 °C for different periods of time and stopped by addition of soybean trypsic inhibitor (SBTI, twice as much in weight as trypsin).

Proteolysis of the ADP/ATP carrier from beef heart either in mitochondria or in inside-out mitochondrial particles (SMP) was carried out under the experimental conditions described in ref *8*.

*Thiol Labeling of Membrane-Embedded Anc2($His_6$)p and Anc2-S161C($His_6$)p.* Suspensions of freshly isolated mitochondria were incubated with CATR or BA under the experimental conditions described for proteolysis experiments. Thiol-containing proteins were then labeled by addition of sulfhydryl reagents, namely, EMA or i-PEO-biotin, at a final concentration of 0.2 mM. The reaction was allowed to process for 30 min at 0 °C in the dark and was terminated by addition of 20 mM DTT. Mitochondrial proteins were then either analyzed by SPAGE or subjected to HTP and IMAC chromatography to purify the HisTag ADP/ATP carrier.

*Purification of Yeast Anc2($His_6$)p.* Purification of Anc2-($His_6$)p was carried out according to the procedure described in ref *12*. Mitochondria were suspended at a final concentration of 10 mg of total mitochondrial protein per mL in a medium made of 0.1 M $Na_2SO_4$, 1 mM EDTA, 10 mM Tris-HCl pH 7.3 and lysed by addition of 1.5% (w/v) DDM followed by 1.5% (w/v) EM. After 5 min of incubation, the soluble fraction was loaded on a HTP column equilibrated in 50 mM $Na_2SO_4$, 1 mM EDTA, 0.1% (w/v) EM, 10 mM Tris-HCl pH 7.3 (1 mL resin/2 mg of total mitochondrial proteins) and the pass-through fraction was collected. As previously reported, it essentially contained three proteins: the ADP/ATP carrier, the phosphate carrier, and mitochondrial porin (*12*). Anc2($His_6$)p was then specifically retained on Ni-NTA resin (Qiagen) in the presence of 5 mM $MgSO_4$, 0.1% (w/v) DDM, 50 mM $Na_2HPO_4$ pH 7.3. After extensive washing of the resin, purified Anc2($His_6$)p was eluted by 500 mM imidazole in 0.1% (w/v) DDM, 50 mM $Na_2HPO_4$ pH 7.3.

*SPAGE and Western-Blotting.* Detergents were removed from protein fractions by overnight precipitation at −20 °C in 80% (v/v) acetone and subsequent washings of the pellets with 10% (v/v) trichloroacetic acid in 50% (v/v) methanol. Proteins were then solubilized in SDS dissociating buffer and separated by SPAGE using 7.5/15% polyacrylamide gels (*23*). Proteins were either stained with Coomassie Brilliant Blue (*24*) or electrotransferred onto a nitrocellulose sheet (*25*). Molecular weights of peptides generated by limited proteolysis of membrane-bound Anc2($His_6$)p were estimated by comparison with standard markers (Rainbow molecular weight markers, Amersham). As indicated, immunodetections of Anc2p fragments were carried out using polyclonal antibodies raised in rabbits against either SDS-treated Anc2p (1/5000 dilution) (*26*) or a 12-residue long peptide corresponding to the C-terminal sequence of Anc2p (1/5000 dilution) (*12*). Anti-aconitase antibodies (*22*) were used at 1/2000 dilution. The immune complexes were detected with EIA-grade HRP conjugate (Bio-Rad, 1/3000 dilution) and HRP was revealed with an ECL reagent kit from Amersham. Peptides carrying the HisTag extension were immunodetected with monoclonal anti-penta His antibodies (Bio-Rad, 1/1000 dilution) and anti-mouse IgG-HRP conjugates (Roche, 1/3000 dilution).

SPAGE of samples resulting from thiol labeling experiments were run in darkness. EMA-labeled proteins were

visualized and photographed under UV light prior to Coomassie Brilliant Blue staining. Proteins labeled by i-PEO-biotin were revealed by immunodetection using an extravidin-HRP conjugate (Sigma-Aldrich, 1/10000 dilution).

*Amino Acid Microsequencing.* After proteolysis, samples of mitochondrial fractions (4 mg of total proteins/mL) were treated with 0.2 M $Na_2CO_3$ (final concentration) pH 11.0 for 30 min at 0 °C, then centrifuged at 100000*g* for 30 min at 0 °C. The supernatant containing soluble proteins was discarded. The membrane protein pellet was resuspended in the sample dissociating buffer and subjected to SPAGE in parallel lanes on the same gel. Proteins were then electroblotted onto PVDF membranes (*25*). One lane was used for immunodetection of the proteolytic peptides, whereas the second one was used for Coomassie Brilliant Blue staining. Stained bands corresponding to immunodetected peptides were excised and submitted to automatic Edman degradation (ABI 492 Procise Sequencer, Perkin-Elmer, Applied Biosystems Division).

*MALDI-TOF and ESI-MSMS Analyses.* Membrane-bound Anc2-S161C($His_6$)p was labeled by i-PEO-biotin and purified by HTP and affinity chromatography as described in preceding sections. The final purified fraction was then precipitated overnight in the presence of 80% (v/v) acetone at −20 °C and solubilized in 1% (w/v) SDS at a protein concentration of about 2 mg/mL. Amino groups were succinylated in the presence of 50 mM succinic anhydride in 200 mM $Na_2CO_3$ pH 8 for 2 h at 20 °C. After a second acetone precipitation, Anc2-S161C($His_6$)p was solubilized in dissociating buffer and subjected to SPAGE. The protein band was detected by Coomassie Blue staining and excised to perform in-gel enzymatic digestion following the procedure previously described by (*27*). Briefly, the gel band containing approximately 10 $\mu$g of protein was successively washed with 25 mM $NH_4HCO_3$ for 15 min and then with 25 mM $NH_4HCO_3$ in 50% (v/v) $CH_3CN$ for 15 min (destaining solutions). This washing cycle was repeated three times and the gel band was finally dried in a vacuum centrifuge. Free thiol groups were reduced in a solution containing 10 mM DTT and 25 mM $NH_4HCO_3$ for 30 min at 37 °C prior to be alkylated by treatment with 55 mM iodoacetamide in 25 mM $NH_4HCO_3$ for 30 min at 37 °C. After extensive washing with the destaining solutions and dehydratation with 100% (v/v) $CH_3CN$, the gel band was dried under vacuum and reswollen in 25 mM $NH_4HCO_3$, 0.1% (w/v) $\beta$-octylglucoside containing trypsin (sequencing grade, Promega, 1/20 w/w trypsin-to-protein ratio). In-gel digestion was allowed to proceed for 5 h at 37 °C. Prior to drying the sample under vacuum, the resulting trypsic peptides were extracted from the gel by passive diffusion using the following solutions: 50% (v/v) $CH_3CN$, then 5% (v/v) formic acid, and finally 100% (v/v) $CH_3CN$. Peptides were solubilized with 1 $\mu$L of 1% (v/v) formic acid, 5 $\mu$L of 10% (w/v) $\beta$-octylglucoside, 1 $\mu$L of 1 M DFP, and 1 mL of 25 mM $NH_4HCO_3$ pH 8. i-PEO-biotin labeled peptides were purified using Avidin-Ultrogel resin (IBF, 50 $\mu$L/$\mu$g of protein): biotinylated peptides retained on the resin were eluted by 30% (v/v) $CH_3CN$ containing 0.4% (v/v) trifluoroacetic acid (TFA).

MALDI-TOF analyses of the sample were carried out in reflector mode. A total of 0.5 $\mu$L of the digest solution was mixed with the same volume of matrix solution (α-cyano-4-hydroxy-trans-cinnamic acid saturated in 60% (v/v) $CH_3CN$, 0.1% (v/v) TFA) and loaded on a target prior to analysis. Mass spectra were recorded on a Autoflex, Bruker Daltonik spectrometer. External calibration was achieved using a mixture of four synthetic peptides (Angiotensin II, Bombesin, ACTH, substance P).

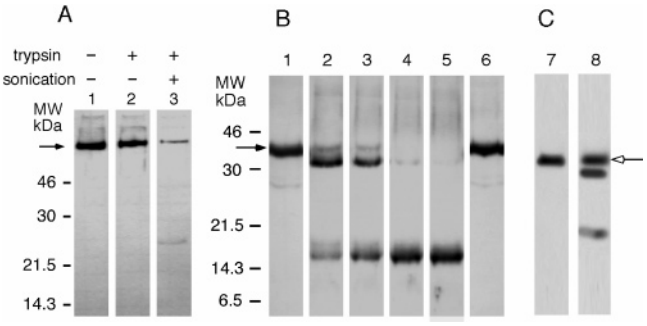


FIGURE 2: Trypsin cleavage of aconitase and of the membrane-embedded ADP/ATP carrier. (A) Intact (lanes 1 and 2) or sonicated (lane 3) mitochondria were incubated for 1 h at 4 °C in the absence (lane 1) or in the presence (lanes 2 and 3) of trypsin. Proteolytic fragments of aconitase were immunodetected using anti-aconitase antiserum (1/2000 dilution). The arrow points to the aconitase band (80 kDa). (B) Time course of the membrane-embedded Anc2($His_6$)p proteolysis by trypsin. Freshly isolated mitochondria were incubated for 10 min at 4 °C in the presence of 20 $\mu$M CATR and then treated with trypsin. Proteolysis was stopped by addition of SBTI (2 mol per mole of trypsin). Proteolytic fragments of the ADP/ATP carrier were immunodetected using anti SDS-denatured Anc2p antiserum (1/5000 dilution). Initial sample without trypsin (lane 1). Mitochondria incubated with trypsin for 30 min (lane 2), 1 h (lane 3), 2 h (lane 4), 4 h (lane 5). Mitochondria incubated for 4 h without trypsin (lane 6). The arrow points to the full-length Anc2($His_6$)p (36 kDa). (C) Trypsin proteolysis of the beef heart carrier. Beef heart mitochondria in the presence of CATR (lane 7) or inside-out particles in the presence of BA (lane 8) were treated with trypsin for 1 h at 4 °C. Proteolytic fragments from the beef carrier were immunodetected using anti SDS-denatured beef carrier antiserum (1/1000 dilution). The white arrow points to the uncleaved beef carrier (30 kDa). In all cases, trypsin was used at a trypsin-to-protein ratio of 1/100 (w/w) under the conditions described in Experimental Procedures. Samples were then lysed with 2% (w/v) SDS and proteins were separated by SPAGE (20 $\mu$g of total protein/lane). After electroblotting onto a nitrocellulose sheet, peptides were allowed to react with the corresponding antisera and immune complexes were detected with ECL reagent.

ESI-MSMS spectra were recorded on a Q-TOF Ultima Waters spectrometer. The dried peptides were resuspended in 0.1% (v/v) formic acid and desalted on a Zip-Tip C18 column (Millipore, UK) prior to be analyzed. Peptides of interest were selected on the basis of their *m*/*z* value and submitted to MSMS fragmentation using specific collision energies.

## RESULTS

*Assessment of Mitochondrial Inner Membrane Tightness.* Topographical approaches should be considered as meaningful only if membrane tightness is demonstrated. Therefore, to avoid possible membrane damage due to freeze thawing, all the experiments described in this paper—limited proteolysis and thiol labeling—were carried out on freshly isolated mitochondria. Mitochondrial inner membrane integrity was checked by the proteolysis due to externally added trypsin of a matrix enzyme, aconitase. As illustrated in Figure 2A (lane 2) aconitase was not cleaved by trypsin treatment of mitochondria in iso-osmotic conditions since it was immunodetected as a single 80 kDa band. In contrast,

when mitochondria were partially disrupted by sonication prior to trypsin treatment, a major 25 kDa proteolysis fragment of aconitase appeared at the expense of the 80 kDa band (lane 3).

As shown hereafter, additional evidence of mitochondria tightness was deduced from experiments carried out on the membrane-embedded ADP/ATP carrier, which demonstrated the conformation-dependent cleavage efficiency of Anc2-($His_6$)p and the differential chemical reactivity of cysteine residues of the carrier to external reagents. Taken together, these results excluded the possibility of mitochondrial membrane leakiness, making relevant the exploration of membrane topography of the ADP/ATP carrier.

*Proteolysis of the Membrane-Embedded Anc2($His_6$)p.* To investigate the topographical changes of the carrier related to conformational changes, proteolysis of membrane-embedded Anc2($His_6$)p with site-specific proteases was carried out on Anc2($His_6$)p-CATR and Anc2($His_6$)p-BA complexes. On the basis of the size and on the immunoreactivity of the resulting fragments toward sequence-directed antibodies, a rough localization of the cleavage sites was deduced. Identification of the proteolysis sites was then ascertained by N-terminal amino acid sequencing of the generated fragments. In contrast to the internal mitochondrial membrane, the external membrane was sufficiently permeabilized during isolation of mitochondria to be crossed by externally added proteases. In screening assays, several site-specific endoproteases, including trypsin, α-chymotrypsin, endoproteinase ArgC, endoproteinase LysC, and endoproteinase GluC, were tested for their ability to cleave the membrane-embedded Anc2($His_6$)p (data not shown). Among them, only trypsin, used under mild conditions, gave reproducible results. The time course of proteolysis by trypsin of the membrane-bound Anc2($His_6$)p-CATR complex is illustrated in Figure 2B. Using a trypsin-to-protein ratio as low as 1/100 (w/w) at 4 °C, only a discrete number of peptides was generated even over a period of 4 h. No cleavage product was detected in a control experiment carried out in the absence of trypsin (lane 6), demonstrating that our mitochondrial preparations were not contamined by endogeneous endoproteases. The 36 kDa band corresponding to the initial carrier was totally digested after 2 h (lanes 2−4). This result was markedly different from that obtained from the proteolysis of the membrane-embedded beef heart ADP/ATP carrier-CATR complex, which remained uncleaved when mitochondria were subjected to similar proteolysis conditions (Figure 2C, lane 7). As discussed below, this finding clearly demonstrates that the peptide segments exposed on both sides of the membrane are not equivalent in the yeast and beef carriers, despite the fact that both proteins display 47% amino acid identity. The cleavage patterns obtained after trypsinolysis of the yeast membrane-bound Anc2($His_6$)p in the presence of either CATR or BA were strikingly different, as illustrated in Figure 3. Cleavage of the Anc2($His_6$)p-CATR complex generated two 34 and 32 kDa fragments together with shorter peptides migrating as a broad band in the 16−18 kDa region (Figure 3A). In contrast, trypsic digestion of the Anc2($His_6$)p-BA complex produced a 34 kDa fragment on one hand and a higher number of 15−17 kDa peptides on the other hand (Figure 3B). This was taken as evidence of conformation-dependent exposure of the peptide chain of the carrier on the cytoplasmic face of the mitochondrial membrane.

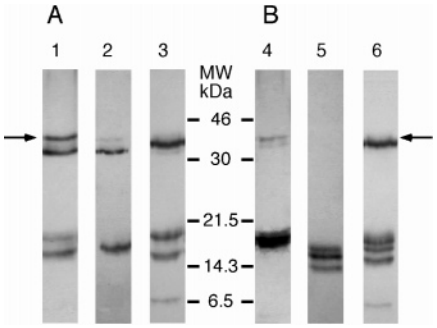


FIGURE 3: Conformation-dependent proteolysis of membrane-embedded Anc2($His_6$)p in mitochondria. Mitochondria in which the ADP/ATP carrier was trapped either in the Anc2($His_6$)p-CATR (A) or Anc2($His_6$)p-BA (B) complex were treated with trypsin for 1h at 4 °C (trypsin-to-protein ratio of 1/100, w/w). Proteolysis products were immunodetected by antibodies directed against the SDS-denaturated Anc2p (lanes 1 and 4), the 12-Cterminal residues of Anc2p (lanes 2 and 5) or the six histidine extension (lanes 3 and 6). SPAGE, Western blot and immunodecoration were performed as described in Experimental Procedures.

*Identification of the Trypsin Cleavage Sites of The Membrane-Embedded Anc2($His_6$)p-CATR Complex.* Fragments originating from the trypsin cleavage of Anc2($His_6$)p-CATR complex (Figure 3A) were characterized according to their reactivity toward either antisera raised against the C-terminal region of the carrier (lane 2) or anti-HisTag antibodies (lane 3). Whereas only weakly reactive toward antibodies directed against the whole protein (lane 1), the 34 kDa peptide was immunodetected by anti-HisTag and therefore arose from a cleavage that occurred in the N-terminal region of Anc2($His_6$)p. In contrast, the 32 kDa peptide reacted with anti-Cter antibodies but not with anti-HisTag antibodies, which indicated it possibly resulted from subsequent cleavage of the 34 kDa with removal of the HisTag sequence. Three peptides were discriminated among the peptides migrating in the 16−18 kDa region based on their distinct immunoreactivity. One of them, approximately 17 kDa MW, reacted with anti-Cter antibodies (lane 2), whereas two others, about 16 and 18 kDa MW were detected with anti-HisTag antibodies (lane 3). As already observed for the 34 kDa peptide, this behavior is paradoxical since the HisTag extension is attached to the C-terminal end of the carrier. This was attributed to the restricted accessibility of the C-terminal region to antibodies compelled by the adjacent HisTag segment since high immunoreactivity of the C-terminal region was demonstrated in control experiments performed with untagged Anc2p (data not shown). Masking of the C-terminal epitope by the HisTag segment probably also explains why uncleaved Anc2($His_6$)p is immunodetected by anti-HisTag antibodies, whereas it only fairly reacts with anti-Cter antibodies.

The finding that some of the released peptides containing the C-terminal region were approximately half of the size of the whole carrier strongly indicated that trypsic cleavage occurred in a central region of the peptide chain. To localize precisely the cleavage sites, the 16−18 kDa fragments were analyzed by N-terminal amino acid sequencing. Two sequences were clearly identified from the analysis of the 16−18 kDa bands: $^{18}$Lys-Glu-Ser-Asn-Phe-Leu-Ile-Asp-Phe-Leu and $^{164}$Gly-Gly-Ala-Arg-Gln-Phe-Asn-Gly-Leu-Ile, which, by

Table 1: Biochemical Characterization of Yeast Strains and Isolated Mitochondria Expressing Anc2($His_6$)p or Anc2-S161C($His_6$)p

| | cells culture[a] | | [$^3$H]ATR binding[b] | | ADP/ATP exchange[c] | |
|---|---|---|---|---|---|---|
| | doubling time (h) | growth yield | $^3$H-ATR (pmol/mg of prot) | $K_d$ (nm) | $K_M^{ADP}$ ($\mu$M) | $V_{max}$ (nmol/min/mg of prot) |
| Anc2($His_6$)p | 4.8 | 9.2 | 450 ± 2 | 270 ± 70 | 4 ± 0.4 | 247 ± 7 |
| Anc2-S161C($His_6$)p | 5.3 | 9.4 | 447 ± 4 | 280 ± 25 | 5.6 ± 1 | 264 ± 14 |

[a] Cells were cultivated at 28 °C, 300 rpm in YPL medium, and kinetic parameters were deduced from $OD_{600\ nm}$. [b] [$^3$H]-ATR binding parameters are calculated from plots shown in Figure 4. [c] ADP/ATP exchange catalyzed by Anc2($His_6$)p or Anc2-S161C($His_6$)p was measured on freshly isolated mitochondria, as described under Experimental Procedures. $V_{max}$ and apparent $K_M$ for external free ADP (evaluated as in ref *20*) were calculated from kinetic data using the Michaelis−Menten equation. The whole values are means of at least three independent experiments.

comparison with the overall sequence of the carrier, allowed us to identify unambiguously the cleavage sites at positions Lys17-Lys18 and Lys163-Gly164. The latter reveals the unexpected accessibility of the matrix m2 loop to externally added trypsin. One of the resulting fragments, spanning Lys18-Lys163, 18 kDa, escaped immunodetection by anti-Cter and anti-HisTag antibodies. The cleavage of the Lys163-Gly164 bond is responsible for the generation of the Gly164-Lys327 peptide, 18 kDa, reactive toward anti-HisTag antibodies and of the Gly164-Lys317 peptide, 17 kDa, reactive toward anti-Cter but not toward anti-HisTag antibodies (see Figure 3A). Besides, cleavage at position Lys17-Lys18 is consistent with the exposure of the N-terminal region to the intermembrane space, as already shown for the bovine protein (*26*) and proposed from genetic engineering approaches (*28*, *29*). Proteolysis experiments also demonstrated the exposure to the intermembrane space of the C-terminal region of Anc2($His_6$)p, therefore affording direct biochemical evidence of a common location of N- and C-terminal extremities of the yeast mitochondrial ADP/ATP carrier on the cytoplasmic side of the membrane in the case of the Anc2($His_6$)p-CATR complex.

*Identification of the Trypsin Cleavage Sites of the Membrane-Embedded Anc2($His_6$)p-BA Complex.* The immunodecoration of cleavage products resulting from the trypsin proteolysis of the Anc2($His_6$)p-BA complex differs from that of the Anc2($His_6$)p-CATR complex, especially in the 15−17 kDa region (Figure 3B). However, the generation from both complexes of a 34 kDa peptide reactive toward anti-HisTag antibodies (lane 6) indicates that a conformation-independent cleavage site is located in the N-terminal region of the carrier. The sequence of the major peptide band immunodetected with anti-Anc2p antibodies in the 15−17 kDa region (lane 4) was ascertained from amino acid analysis: $^{179}$Thr-Leu-Lys-Ser-Asp-Gly-Val-Ala-Gly-Leu-Tyr-Arg-Gly-Phe-Leu, indicating that cleavage of the carrier occurred at the Lys178-Thr179 bond. Interestingly, although distinct from that accessible in the case of Anc2($His_6$)p-CATR complex (Lys163-Gly164), this peptide bond is also located in the m2 loop of the carrier.

Results from proteolysis experiments were taken as evidence that the m2 loop of the membrane-embedded carrier, whereas predicted to face the matrix, inserts to some extent into the membrane in a conformation-dependent manner. Because this result was unexpected, we sought to probe the dynamics of the m2 loop by site-specific chemical modification of a cysteine residue. Thus, we constructed a mutant of the Anc2p carrier in which a cysteine residue was introduced by site-directed mutagenesis to replace serine 161 in the m2 loop, the Ser/Cys substitution being chosen to minimize steric effects. We then investigated the accessibility to SH reagents of Cys 161 of the mutated carrier Anc2-S161C($His_6$)p.

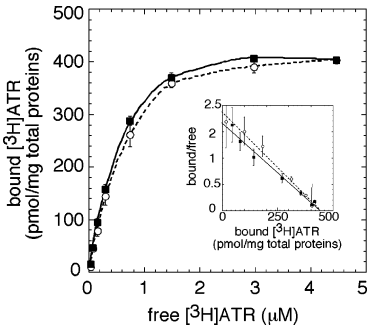


FIGURE 4: Specific binding of [$^3$H]ATR to mitochondria expressing Anc2($His_6$)p or Anc2-S161C($His_6$)p. Freshly isolated mitochondria (1 mg of total protein) from yeast cells expressing either Anc2-($His_6$)p (white circles) or Anc2-S161C($His_6$)p (black squares) were incubated with increasing concentrations of [$^3$H]ATR in 1 mL of a standard medium (120 mM KCl, 1 mM EDTA, 10 mM Tris pH 7.4) for 45 min at 0 °C. After centrifugation, the radioactivity associated with the mitochondrial pellet was estimated by scintillation counting. Data were corrected for unspecific binding from parallel experiments carried out in the presence of 20 $\mu$M CATR. The inset shows the Scatchard plot of the binding data. Error bars were calculated from three independent experiments.

*Functional Characterization of Anc2-S161C($His_6$)p Mutant.* To ensure that Anc2-S161C($His_6$)p was functional, the corresponding mutated gene was used to transform the JL1-3-1B strain, which is unable to grow on a nonfermentable carbon source. Transformants were able to grow on glycerol or lactate, indicating that the mutated gene encoded an active ADP/ATP carrier. The strains expressing Anc2($His_6$)p or Anc2-S161C($His_6$)p were grown at 28 °C in liquid media using lactate as a carbon source. As shown in Table 1, both strains displayed very similar growth characteristics with doubling times of about 5 h and $OD_{600}$ values of the cultures at the growth plateau of about 9.

The amounts of Anc2($His_6$)p and Anc2-S161C($His_6$)p in the corresponding mitochondria were similar, as evaluated roughly by Western blotting after SPAGE of mitochondrial lysates (data not shown). A more accurate determination of carrier content was performed by binding experiments of radiolabeled atractyloside, a specific inhibitor of the ADP/ATP carrier. As shown in Figure 4, binding of [$^3$H]-ATR increased as a function of added ligand and reached a plateau, following similar curves for mitochondria expressing Anc2-($His_6$)p or Anc2-S161C($His_6$)p. From the Scatchard plots (Figure 4, inset), identical $K_d$ values (280 nM) and equal number of binding sites (450 pmol [$^3$H]-ATR/mg of mitochondrial protein) were calculated for both variants of the carrier (Table 1). These results indicated that introduction

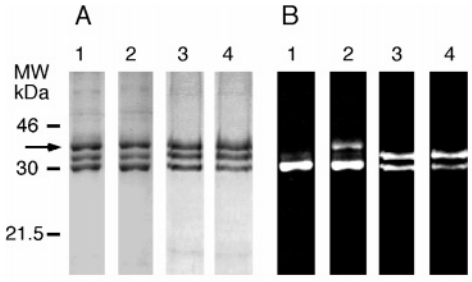


FIGURE 5: EMA labeling of the membrane-bound ADP/ATP carrier in yeast mitochondria. Freshly isolated mitochondria expressing Anc2($His_6$)p or Anc2-S161C($His_6$)p were first incubated with either CATR or BA prior to be treated with 200 $\mu$M EMA for 30 min at 0 °C in darkness. The samples were then solubilized by treatment with a DDM/Emulphogen (1/1, w/w) mixture and subjected to HTP chromatography (see Experimental Procedures). Proteins contained in the pass-through fraction (ADP/ATP carrier, Pi carrier and porin) were separated by SPAGE and vizualized by either Coomassie blue staining (A) or by irradiation under UV-light that revealed the presence of EMA (B). Lane 1, Anc2($His_6$)p-CATR; lane 2, Anc2-S161C($His_6$)p-CATR; lane 3, Anc2($His_6$)p-BA; lane 4, Anc2-S161C($His_6$)p-BA. The arrow points to Anc2($His_6$)p.

of the Ser/Cys mutation into Anc2($His_6$)p did not significantly modify either the amount of carrier in mitochondria or its binding affinity for atractyloside.

ADP/ATP exchange activities of Anc2($His_6$)p and Anc2-S161C($His_6$)p in corresponding mitochondria were measured by the luciferase/luciferin system (see Experimental Procedures). Variation of the exchange rate as a function of ADP concentration was analyzed with the Michaelis−Menten equation. As shown in Table 1, Anc2($His_6$)p and Anc2-S161C($His_6$)p exhibit very similar $K_M$ and $V_{max}$ values, thus indicating that the introduction of an exogenous cysteine residue at position 161 neither impairs the binding of nucleotides nor affects ADP/ATP transport efficiency.

The similar properties of Anc2($His_6$)p and Anc2-S161C-($His_6$)p regarding atractyloside binding and ADP/ATP transport strongly suggested that the two variants of the carrier adopted the same fold in the mitochondrial membrane. This was confirmed by trypsin digestion experiments carried out as described in the legend of Figure 5, which led to similar proteolytic patterns for Anc2($His_6$)p and Anc2-S161C($His_6$)p (data not shown).

*EMA Labeling of the Membrane-Embedded Anc2($His_6$)p.* Eosin-5-maleimide (EMA) was used as a covalent, membrane-impermeable thiol reagent to probe the accessibility of the m2 loop from the cytosolic face of the membrane. Preliminary experiments were carried out with wild-type membrane-bound Anc2($His_6$)p-CATR carrier complex by incubating mitochondria in the presence of 200 $\mu$M EMA for 30 min at 0 °C. Proteins were then solubilized in a DDM/Emulphogen (1/1, w/w) detergent mixture and subjected to HTP chromatography (see Experimental Procedures). As illustrated in Figure 5A, lane 1, the pass-through fraction contained three proteins that were detected by Coomassie Blue staining. As previously reported, they corresponded to the ADP/ATP carrier (MW 36 kDa), the phosphate carrier (MW 32 kDa), and the mitochondrial porin (MW 30 kDa) (*12*). Examination of the gel under UV light showed that only two proteins were rendered fluorescent upon incorporation of EMA (Figure 5B, lane 1). The protein that failed to react with EMA was clearly identified as the ADP/ATP carrier by Western blotting using anti-Anc2p antibodies (not shown). Inaccessibility of cysteine residues of the membrane-bound ADP/ATP carrier to EMA added outside mitochondria was taken as an evidence of mitochondria tightness since the carrier could be labeled when the mitochondrial suspension was subjected to sonication prior to EMA labeling, i.e., because of membrane disruption and consequently exposure of matrix cysteine residues to the reagent (data not shown).

*EMA Labeling of the Membrane-Embedded Anc2-S161C-($His_6$)p.* Exposure of the central loop of Anc2p to the intermembrane space was assessed by comparison of the extent of EMA labeling of Anc2($His_6$)p with that of Anc2-S161C($His_6$)p. Unlike Anc2($His_6$)p-CATR (Figure 5B, lane 1), Anc2-S161C($His_6$)p-CATR incorporated EMA when subjected to a similar labeling procedure (Figure 5B, lane 2). Since the two variants of the carrier only differ by the presence of Cys161 in Anc2-S161C($His_6$)p, it is inferred that this residue is the target of EMA. As presented in the following section, additional experiments based on chemical cleavage of thiol-labeled Anc2-S161C($His_6$)p and mass spectrometry determinations have been devised to confirm this result.

Endogenous cysteine residues of Anc2($His_6$)p are not accessible to EMA from the intermembrane space, irrespective of the conformational state of the membrane-bound carrier: no labeling was observed in the presence of either CATR or BA (Figure 5B, lanes 1 and 3). In contrast, labeling of Cys 161 was conformation-sensitive, as EMA alkylated this residue in the Anc2-S161C($His_6$)p-CATR complex (lane 2) but not in the Anc2-S161C($His_6$)p-BA complex (lane 4), thus confirming topographical changes of the m2 loop inherent in the conformational transition of the carrier.

*Localization of the Reaction Site of The Thiol Reagents.* Because of the presence in Anc2p of four endogenous Cys residues, located at positions 72, 243, 270, and 287 (see Figure 1) control mapping experiments were carried out to ascertain that labeling by EMA of the Anc2-S161C($His_6$)p-CATR complex was exclusively directed to cysteine 161. Therefore, the protein band corresponding to EMA-labeled Anc2-S161C($His_6$)p-CATR was isolated by SPAGE and in-gel digested by trypsin for MALDI-TOF-MS analyses (see Experimental Procedures). However, attempts to detect trypsic peptides carrying EMA on the basis of their implemented *m*/*z* values were unsuccessful, probably due to the instability of this reagent (*30*). Therefore, a more suitable thiol reagent, i-PEO-biotin, was used to achieve MALDI-TOF-MS analyses. As EMA, this thiol-specific reagent is membrane-impermeable (*31*) and it covalently binds to membrane-embedded Anc2-S161C($His_6$)p-CATR complex whereas reacting neither with Anc2($His_6$)p-CATR nor with Anc2-S161C($His_6$)p-BA and Anc2($His_6$)p-BA (data not shown).

The trypsic peptides generated from in-gel digestion of Anc2-S161C($His_6$)p labeled with i-PEO-biotin were analyzed by MALDI-TOF mass spectrometry. It should be recalled that SH groups that did not react with i-PEO-biotin were alkylated with iodoacetamide (see Experimental Procedures). Therefore, cysteine-containing peptides were detected according to their *m*/*z* values when alkyled by either i-PEO-biotin (+414.2 Da per Cys residue) or iodoacetamide (+57 Da per Cys residue) (Table 2). MALDI-TOF analysis of the trypsic digest of Anc2-S161C($His_6$)p is shown in Figure 6.

Table 2: Characteristics of the Cys-Containing Peptides Generated from In-Gel Trypsinolysis of Anc2-S161C($His_6$)p Labeled by i-PEO-biotin[a]

| Cys no.[b] | trypsic fragment[c] | native average mass (Da)[d] | *m*/*z* of peptides alkylated by i-PEO-biotin[e] | *m*/*z* of peptides alkylated by iodoacetamide[f] |
|---|---|---|---|---|
| 72 | 65−75 | 1513.73 | 1927.93 | 1570.73 |
| 161 | 154−167 | 1691.74 | 2105.94 | 1748.74 |
| 243 | 204−251 | 5246.62 | 5660.82 | 5303.62 |
| 270 | 254−272 | 2223.94 | 2638.14 | 2280.94 |
| 287 | 273−293 | 2303.20 | 2717.40 | 2360.20 |

[a] Membrane-embedded Anc2-S161C($His_6$)p-CATR complex was labeled by i-PEO-biotin and purified as described under Experimental Procedures. The sample was succinylated and subjected to SPAGE. The protein band was stained with Coomassie blue then excised and treated by iodoacetamide to alkylate the remaining unreacted cysteine residues. After in-gel digestion with trypsin, peptides were extracted from the gel and analyzed by MALDI-TOF-MS (see Figure 6). Theoretical masses of peptides were calculated with average isotopic abundancies. [b] The sequence of Anc2($His_6$)p was numbered taking into account the absence of Met residue at the N-terminal extremity (*11*). [c] Trypsin only cleaved the polypeptidic chain at the C-ter of Arg residues since Lys residues were succinylated. [d] Masses of peptides were incremented with 100 Da per Lys residue present corresponding to the addition of succinyl groups. [e,f] Modification of a Cys residue by either i-PEO-biotin or iodoacetamide results in a mass implementation of 414.2 or 57 Da, respectively.

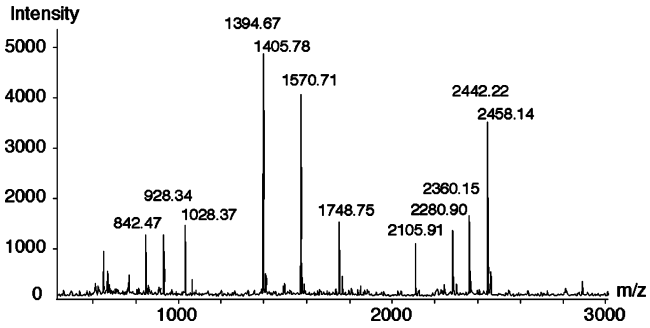


FIGURE 6: MALDI-TOF mass spectrum of Anc2-S161C($His_6$)p fragments covalently labeled by i-PEO-biotin. Membrane-embedded Anc2-S161C($His_6$)p-CATR was incubated in the presence of i-PEO-biotin, then purified and subjected to in-gel trypsinolysis (see Experimental Procedures). Released peptides were analyzed by MALDI-TOF and fragments containing cysteine residues were identified according to their expected masses (see Table 2).

Peptides containing Cys72, Cys270, and Cys287 were clearly identified under the corresponding forms alkylated by iodoacetamide, at *m*/*z* values of 1570.7, 2280.9, and 2360.2, respectively, whereas they were not detected as alkylated by i-PEO-biotin. On the contrary, the 154−167 peptide was simultaneously detected under the form alkylated by i-PEO-biotin and that alkylated by iodoacetamide at the characteristic *m*/*z* values of 2105.9 and 1748.7, respectively.

For additional characterization, the 154−167 peptide was purified from a trypsin digest of Anc2-S161C($His_6$)p-CATR prelabeled with i-PEO-biotin, using affinity chromatography with immobilized avidin. The amino acid sequence of this fragment was determined by ESI-MSMS analysis: Leu-Ala-Ala-Asp-Ser-Lys-Ser-Cys-Lys-Lys-Gly-Gly-Ala-Arg, demonstrating unambiguously that the cysteine residue located at position 161 was labeled by i-PEO-biotin.

The trypsic peptide 204−251, containing Cys243, could not be resolved by MALDI-TOF, because of its too high *m*/*z* value (Table 2). An alternative approach was to check for the presence of i-PEO-biotin, possibly combined to Cys243, in appropriate fragments of the carrier, using a sensitive detection method. We took advantage of the existence in the sequence of Anc2p of a single Asn170-Gly171 bond which is cleavable by hydroxylamine, releasing two peptides, 17 and 18.5 kDa MW (*11*). Peptides were separated by SPAGE then electroblotted onto nitrocellulose and i-PEO-biotin labeling was detected by extravidine-HRP conjugate and ECL system. Only the N-terminal 1−170 region of Anc2-S161C($His_6$)p was reactive, ruling out the possibility that Cys243 as Cys270 and Cys287 could be labeled by i-PEO-biotin (data not shown).

## DISCUSSION

This paper reports on the exploration of the dynamic topography of the membrane-embedded yeast mitochondrial ADP/ATP carrier. Two independent approaches were used: (i) limited proteolysis by trypsin, followed by identification of the cleavage sites by immunodetection and microsequencing of the generated fragments, and (ii) assessment of the accessibility of a matrix-facing cysteine to externally added, nonpermeable thiol alkylating reagents. Both approaches were carried out on mitochondria isolated from a genetically modified *S. cerevisiae* strain that only expressed the isoform 2 of the ADP/ATP carrier. This isoform is the only one of the three present in *S. cerevisiae* that is essential for growth of the cells on a nonfermentable carbon source (*32*). Experiments were performed on mitochondria preincubated with either CATR or BA, two potent specific inhibitors of ADP/ATP transport. This relies on the previous finding that CATR and BA lock two distinct conformations of the carrier involved in the transport process.

*Proteolysis of the Yeast Mitochondrial ADP/ATP Carrier with Trypsin.* To overcome possible drawbacks inherent to uncontrolled membrane integrity, mitochondria tightness was carefully checked. This was assessed by the fact that aconitase used as a control protein since it is located in the matrix compartment was not cleaved by external trypsin, even under experimental conditions that allowed extensive digestion of the ADP/ATP carrier. In addition, only after sonication of mitochondria could the carrier be labeled by EMA, a thiol specific reagent.

Trypsin cleavage of Anc2($His_6$)p trapped in CATR-carrier complex (36 kDa) occurred after short periods of incubation, generating 32−34 kDa and 16−18 kDa fragments. The latter accumulated at the expense of 32−34 kDa peptides when the proteolysis was lengthened, without being further digested. Some peptides migrating in the 16−18 kDa region were reactive toward anti-Cter or anti-HisTag antibodies, leading to the conclusion that they could only result from a cleavage occurring in the central region of the peptide chain of the carrier, i.e., in the m2 loop (see Figure 1). A cleavage site was indeed identified at the Lys163-Gly164 bond by microsequencing. Interestingly, the trypsic attack of the Anc2($His_6$)p-BA complex also occurred in the m2 loop but at the Lys178-Thr179 bond. This result demonstrated the conformation-dependent accessibility to externally added trypsin of the m2 loop despite the fact that it is postulated to face the matrix compartment (see Figure 1).

*Cysteine Labeling Studies.* The unexpected proteolytic cleavage of the m2 loop of the yeast carrier led us to further investigate its topographical dynamics by thiol specific

labeling. For this purpose, we constructed and characterized the fully functional Anc2-S161C($His_6$)p mutant in which a cysteine residue was introduced in the m2 loop at position 161. It is noteworthy that we decided not to introduce the S161C mutation into a Cys-less protein, since the four endogenous cysteine residues of Anc2($His_6$)p are not reactive toward externally added thiol reagents (*9*). Furthermore, retaining the native cysteine probably favors the functional state of the carrier, as demonstrated by the essential role of cysteine residues with regard to the lipid-mediated dimerization of the carrier (*33*). The conformation-dependent accessibility of Cys161 was evaluated by assessing its reactivity toward the membrane-impermeable thiol reagent eosin-5-maleimide (EMA) in CATR- and BA-carrier complexes in mitochondria. Only in the CATR-carrier complex could EMA added outside mitochondria react with Cys161, consistent with our finding of the conformation-dependent unmasking of a discrete segment of the m2 loop. MALDI-TOF analyses ascertained that Cys161 was the sole cysteine residue to be labeled by thiol reagent, confirming the inaccessibility of cysteine residues located at positions 72, 243, 270, and 287 (*9*).

Both approaches described in the present work support the conclusion that the segment spanning residues 156−192 of the yeast ADP/ATP carrier intrudes to some extent into the mitochondrial inner membrane, in a conformation-sensitive manner.

*How Can the Re-Entrant m2 Loop Be Reconciled with the Crystallographic Bovine Structure?* We recently determined the structure at 2.2 Å resolution of the bovine isoform 1 ADP/ATP carrier by X-ray crystallography (*5*). In agreement with the tripartite structure noted from the sequence analysis of mitochondrial carriers (*3*), the crystallographic structure of the ADP/ATP carrier shows three motifs that are similarly folded. Each of them consists of one odd- and one even-numbered transmembrane α-helix connected to each other by a 32−34-residue long loop, which is exposed to the matrix compartment. Connecting loops each contain a 12-residue long α-helix located parallel to the membrane plane that is attached to the odd- and to the even-numbered helix through a 15- and a 10-residue-long random-coil, respectively. Yeast Anc2p and beef isoform 1 ADP/ATP carriers share 47% sequence identity, thus strongly supporting similar folding of both carriers. In the bovine crystal structure, which is a CATR-carrier complex, matrix loops do not intrude into the membrane. An alternative interpretation of the results presented in this study relies on the fact that the ADP/ATP carrier in complex with CATR was crystallized as a monomer, although many biochemical approaches demonstrated that it forms dimers, with one CATR molecule bond per carrier dimer (*34*−*37*). Therefore, the finding that CATR binds inside the cavity of a carrier monomer implies the existence of an asymmetric dimeric CATR-carrier complex consisting of the association of strongly interacting but probably structurally different monomers. Whereas it is likely that each carrier monomer contains one six-transmembrane α-helix bundle, the overall arrangement of transmembrane helices and of connecting flexible loops in two associated monomers would be different. Therefore, the m2 loop shown in the present work to intrude into the membrane most probably belongs to the monomer that is not carrying the CATR molecule. The association of distinct interacting monomeric conformers of the carrier to constitute functional dimers would be consistent with the existence of two nucleotide specific binding sites per carrier dimer located on each face of the membrane (*38*). In this model, negative interactions between two internal or two external sites and positive interactions between internal and external sites of different monomers would favor the concomitant binding to the transport unit of one nucleotide coming from the intermembrane space and of one coming from the matrix.

*Conformational States of the Central Loop m2.* As demonstrated in the present work, the m2 loop undergoes significant topographical changes when the carrier is trapped by either CATR or BA, illustrating its functional dynamics. Similar conclusions were drawn from limited proteolysis experiments carried out on the membrane-bound beef ADP/ATP carrier (*8*). It was shown that the carrier could be cleaved by proteases in inverted submitochondrial particles under in the BA-carrier complex, whereas no proteolytic cleavage occurred in the CATR-carrier complex (see Figure 2C, lanes 7 and 8). In particular, one conformation-sensitive cleavage site was localized at Lys146-Gly147 bond, which belongs to the matrix m2 loop leading to the proposal that masking/unmasking of discrete regions of this loop are related to the dynamics of the carrier.

Another striking feature of the m2 loop of the ADP/ATP carrier resides in its central role for substrate recognition as assessed by photolabeling approaches (*7*, *39*). In yeast mitochondria, a restricted sequence of Anc2p spanning Ser182-Arg191, adjacent to the trypsic cleavage sites identified in this study, was photolabeled by azido-naphthoyl-ADP (*11*). Taken together, these results strongly suggest an involvement of the m2 loop in the nucleotide translocation pathway and therefore its possible role in the functioning of ADP/ATP transport.

The sidedness of SH groups in the membrane-embedded beef heart ADP/ATP carrier has been probed following their chemical modification by thiol-specific reagents, either in mitochondria or in submitochondrial inverted particles (*40*). No significant labeling of the carrier by membrane-impermeable EMA occurred in mitochondria, whereas cysteine residues were reactive in inside-out particles. Three cysteine residues out of four present in the sequence of the bovine carrier could be alkylated by EMA, thus demonstrating the accessibility of loops m1, m2, and m3 from the matrix compartment. On the basis of differential chemical reactivities of cysteine residues toward *N*-ethylmaleimide and EMA, the authors suggested that the m1 loop is exposed to the matrix compartment, whereas the m3 loop, and to a lesser extent the m2 loop, intrude into the membrane (*10*). Models of the ADP/ATP carrier showing matrix-exposed loops protruding into the membrane have been proposed from chemical labeling studies (*1*). Recently, Terada and co-workers used a cysteine-scanning approach to probe CATR- and BA-induced conformation changes of the yeast carrier (*41*, *42*), but no conformational change of the m2 loop of the yeast carrier has been reported so far. From studies performed on the beef heart carrier, Terada and co-workers attributed restricted roles to matrix loops. According to their interpretations, loop m1 functions as a gate for the transport and loop m2 is restricted to nucleotide binding (*10*). Whereas we have previously demonstrated that the m2 loop carries an ADP/ATP recognition site (*11*), we propose on the basis

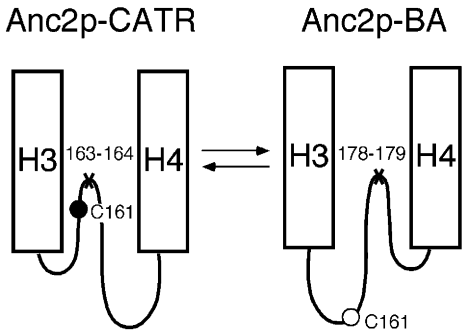


FIGURE 7: Conformations of the m2 loop of the yeast ADP/ATP carrier. Schematic model of the conformational changes undergone by the m2 loop when the carrier shifts from the CATR- to the BA-carrier complexes, as deduced from the results presented in this work. Crosses refer to the peptidic bonds reached by trypsin. The exogeneous cysteine residue introduced at position 161 is highlighted by a circle colored in black when it is accessible to thiol reagents added from outside or in white when it is not.

of the results presented here that it also actively participates to the nucleotide translocation through a swinging movement (Figure 7).

Moreover, the implication of flexible loops connecting transmembrane helices has been proposed in the case of several transmembrane systems. Hence, the existence of a re-entrant loop in the mitochondrial carnitine/acylcarnitine carrier has been reported recently (*43*). This carrier belongs to the mitochondrial carrier family and is therefore postulated to consist of six transmembrane α-helices. From the exploration of the topography of this carrier, performed using single cysteine mutants, it was demonstrated that Cys136 was accessible to nonpermeable thiol reagents added outside mitochondria. Similar to the findings presented in the present study, this residue belongs to the matrix loop m2 of the carnitine/acylcarnitine carrier, therefore suggesting that this loop takes part of the substrate translocation path. Re-entrant loops involved in substrate binding have also been identified by biochemical approaches, both for potassium channels (*44*) and for the glutamate transporter (*45*). Their occurrence was confirmed by the elucidation of the high-resolution structures of the corresponding proteins (*46*, *47*).

## ACKNOWLEDGMENT

We thank Carine De Marcos-Lousa and Véronique Trézéguet (IBGC-CNRS, Bordeaux, France) for the gifts of anti-aconitase antibodies, yeast strain and plasmid. We thank Jean-Pierre Andrieu (IBS, Grenoble, France) and Françoise Schöentgen (CNRS, Orléans, France) for expert amino acid analyses. We are grateful to Jérôme Garin for his help in mass spectra analyses.

## REFERENCES

1. Klingenberg, M. (1993) Dialectics in carrier research: the ADP/ATP carrier and the uncoupling protein, *J. Bioenerg. Biomembr. 25*, 447−457.
2. Fiore, C., Trézéguet, V., Le Saux, A., Roux, P., Schwimmer, C., Dianoux, A. C., Noël, F., Lauquin, G. J.-M., Brandolin, G., and Vignais, P. V. (1998) The mitochondrial ADP/ATP carrier: structural, physiological and pathological aspects, *Biochimie 80*, 137−150.
3. Walker, J. E., and Runswick, M. J. (1993) The mitochondrial transport protein superfamily, *J. Bioenerg. Biomembr. 25*, 435−446.
4. Dahout-Gonzalez, C., Brandolin, G., and Pebay-Peyroula, E. (2003) Crystallization of the bovine ADP/ATP carrier is critically dependent upon the detergent-to-protein ratio, *Acta Crystallogr. D Biol. Crystallogr. 59*, 2353−2355.
5. Pebay-Peyroula, E., Dahout-Gonzalez, C., Kahn, R., Trézéguet, V., Lauquin, G. J.-M., and Brandolin, G. (2003) Structure of mitochondrial ADP/ATP carrier in complex with carboxyatractyloside, *Nature 426*, 39−44.
6. Boulay, F., Lauquin, G. J.-M., Tsugita, A., and Vignais, P. V. (1983) Photolabeling approach to the study of the topography of the atractyloside binding site in mitochondrial adenosine 5′-diphosphate/adenosine 5′-triphosphate carrier protein, *Biochemistry 22*, 477−484.
7. Dalbon, P., Brandolin, G., Boulay, F., Hoppe, J., and Vignais, P. V. (1988) Mapping of the nucleotide-binding sites in the ADP/ATP carrier of beef heart mitochondria by photolabeling with 2-azido[alpha-32P]adenosine diphosphate, *Biochemistry 27*, 5141−5149.
8. Marty, I., Brandolin, G., Gagnon, J., Brasseur, R., and Vignais, P. V. (1992) Topography of the membrane-bound ADP/ATP carrier assessed by enzymatic proteolysis, *Biochemistry 31*, 4058−4065.
9. Hatanaka, T., Kihira, Y., Shinohara, Y., Majima, E., and Terada, H. (2001) Characterization of loops of the yeast mitochondrial ADP/ATP carrier facing the cytosol by site-directed mutagenesis, *Biochem. Biophys. Res. Commun. 286*, 936−942.
10. Terada, H., and Majima, E. (1997) Important role of loops in the transport activity of the mitochondrial ADP/ATP carrier., *Prog. Colloid Polym. Sci. 106*, 192−197.
11. Dianoux, A. C., Noël, F., Fiore, C., Trézéguet, V., Kieffer, S., Jaquinod, M., Lauquin, G. J.-M., and Brandolin, G. (2000) Two distinct regions of the yeast mitochondrial ADP/ATP carrier are photolabeled by a new ADP analogue: 2-azido-3′−O-naphthoyl-[β-32P]ADP. Identification of the binding segments by mass spectrometry, *Biochemistry 39*, 11477−11487.
12. Fiore, C., Trézéguet, V., Roux, P., Le Saux, A., Noël, F., Schwimmer, C., Arlot, D., Dianoux, A. C., Lauquin, G. J.-M., and Brandolin, G. (2000) Purification of histidine-tagged mitochondrial ADP/ATP carrier: influence of the conformational states of the C-terminal region, *Protein Expr. Purif. 19*, 57−65.
13. Ashani, Y., and Catravas, G. N. (1980) Highly reactive impurities in Triton X-100 and Brij 35: partial characterization and removal, *Anal. Biochem. 109*, 55−62.
14. Brandolin, G., Meyer, C., Defaye, G., Vignais, P. M., and Vignais, P. V. (1974) Partial purification of an atractyloside-binding protein from mitochondria, *FEBS Lett. 46*, 149−153.
15. Lauquin, G. J.-M., and Vignais, P. V. (1976) Interaction of ($^3$H) bongkrekic acid with the mitochondrial adenine nucleotide translocator, *Biochemistry 15*, 2316−2322.
16. Drgon, T., Sabova, L., Nelson, N., and Kolarov, J. (1991) ADP/ATP translocator is essential only for anaerobic growth of yeast *Saccharomyces cerevisiae*, *FEBS Lett. 289*, 159−162.
17. Gietz, R. D., and Schiestl, R. H. (1991) Applications of high efficiency lithium acetate transformation of intact yeast cells using single-stranded nucleic acids as carrier, *Yeast 7*, 253−263.
18. Daum, G., Bohni, P. C., and Schatz, G. (1982) Import of proteins into mitochondria. Cytochrome *b*2 and cytochrome *c* peroxidase are located in the intermembrane space of yeast mitochondria, *J. Biol. Chem. 257*, 13028−13033.
19. Brandolin, G., Le Saux, A., Trézéguet, V., Vignais, P. V., and Lauquin, G. J.-M. (1993) Biochemical characterisation of the isolated Anc2 adenine nucleotide carrier from *Saccharomyces cerevisiae* mitochondria, *Biochem. Biophys. Res. Commun. 192*, 143−150.
20. Dassa, E. P., Dahout-Gonzalez, C., Dianoux, A. C., and Brandolin, G. (2005) Functional characterization and purification of a *Saccharomyces cerevisiae* ADP/ATP carrier-iso 1 cytochrome *c* fusion protein, *Protein Expr. Purif. 40*, 358−369.
21. Lyman, G. E., and DeVincenzo, J. P. (1967) Determination of picogram amounts of ATP using the luciferin-luciferase enzyme system, *Anal. Biochem. 21*, 435−443.
22. De Marcos Lousa, C., Trézéguet, V., Dianoux, A. C., Brandolin, G., and Lauquin, G. J.-M. (2002) The human mitochondrial ADP/ATP carriers: kinetic properties and biogenesis of wild-type and mutant proteins in the yeast *S. cerevisiae*, *Biochemistry 41*, 14412−14420.
23. Laemmli, U. K. (1970) Cleavage of structural proteins during the assembly of the head of bacteriophage T4, *Nature 227*, 680−685.

24. Diezel, W., Kopperschlager, G., and Hofmann, E. (1972) An improved procedure for protein staining in polyacrylamide gels with a new type of Coomassie Brilliant Blue, *Anal. Biochem. 48*, 617−620.
25. Towbin, H., Staehelin, T., and Gordon, J. (1979) Electrophoretic transfer of proteins from polyacrylamide gels to nitrocellulose sheets: procedure and some applications, *Proc. Natl. Acad. Sci. U.S.A. 76*, 4350−4354.
26. Brandolin, G., Boulay, F., Dalbon, P., and Vignais, P. V. (1989) Orientation of the N-terminal region of the membrane-bound ADP/ATP carrier protein explored by antipeptide antibodies and an arginine-specific endoprotease. Evidence that the accessibility of the N-terminal residues depends on the conformational state of the carrier, *Biochemistry 28*, 1093−1100.
27. Rabilloud, T., Kieffer, S., Procaccio, V., Louwagie, M., Courchesne, P. L., Patterson, S. D., Martinez, P., Garin, J., and Lunardi, J. (1998) Two-dimensional electrophoresis of human placental mitochondria and protein identification by mass spectrometry: toward a human mitochondrial proteome, *Electrophoresis 19*, 1006−1014.
28. Hatanaka, T., Hashimoto, M., Majima, E., Shinohara, Y., and Terada, H. (1999) Functional expression of the tandem-repeated homodimer of the mitochondrial ADP/ATP carrier in *Saccharomyces cerevisiae*, *Biochem. Biophys. Res. Commun. 262*, 726−730.
29. Trézéguet, V., Le Saux, A., David, C., Gourdet, C., Fiore, C., Dianoux, A., Brandolin, G., and Lauquin, G. J.-M. (2000) A covalent tandem dimer of the mitochondrial ADP/ATP carrier is functional in vivo, *Biochim. Biophys. Acta 1457*, 81−93.
30. Majima, E., Goto, S., Hori, H., Shinohara, Y., Hong, Y. M., and Terada, H. (1995) Stabilities of the fluorescent SH-reagent eosin-5-maleimide and its adducts with sulfhydryl compounds, *Biochim. Biophys. Acta 1243*, 336−342.
31. Muroi, M., Ohnishi, T., and Tanamoto, K. (2002) Regions of the mouse CD14 molecule required for toll-like receptor 2- and 4-mediated activation of NF-kappa B, *J. Biol. Chem. 277*, 42372−42379.
32. Kolarov, J., Kolarova, N., and Nelson, N. (1990) A third ADP/ATP translocator gene in yeast, *J. Biol. Chem. 265*, 12711−12716.
33. Dyall, S. D., Agius, S. C., De Marcos Lousa, C., Trézéguet, V., and Tokatlidis, K. (2003) The dynamic dimerization of the yeast ADP/ATP carrier in the inner mitochondrial membrane is affected by conserved cysteine residues, *J. Biol. Chem. 278*, 26757−26764.
34. Block, M. R., Zaccai, G., Lauquin, G. J.-M., and Vignais, P. V. (1982) Small angle neutron scattering of the mitochondrial ADP/ATP carrier protein in detergent, *Biochem. Biophys. Res. Commun. 109*, 471−477.
35. Hackenberg, H., and Klingenberg, M. (1980) Molecular weight and hydrodynamic parameters of the adenosine 5′-diphosphate−adenosine 5′-triphosphate carrier in Triton X-100, *Biochemistry 19*, 548−555.
36. Klingenberg, M., Riccio, P., and Aquila, H. (1978) Isolation of the ADP, ATP carrier as the carboxyatractylate protein complex from mitochondria, *Biochim. Biophys. Acta 503*, 193-210.
37. Riccio, P., Aquila, H., and Klingenberg, M. (1975) Purification of the carboxy-atractylate binding protein from mitochondria, *FEBS Lett. 56*, 133−138.
38. Block, M. R., and Vignais, P. V. (1984) Substrate-site interactions in the membrane-bound adenine-nucleotide carrier as disclosed by ADP and ATP analogs, *Biochim. Biophys. Acta 767*, 369−376.
39. Mayinger, P., Winkler, E., and Klingenberg, M. (1989) The ADP/ATP carrier from yeast (AAC-2) is uniquely suited for the assignment of the binding center by photoaffinity labeling, *FEBS Lett. 244*, 421−426.
40. Majima, E., Koike, H., Hong, Y. M., Shinohara, Y., and Terada, H. (1993) Characterization of cysteine residues of mitochondrial ADP/ATP carrier with the SH-reagents eosin 5-maleimide and *N*-ethylmaleimide, *J. Biol. Chem. 268*, 22181−22187.
41. Kihira, Y., Iwahashi, A., Majima, E., Terada, H., and Shinohara, Y. (2004) Twisting of the second transmembrane alpha-helix of the mitochondrial ADP/ATP carrier during the transition between two carrier conformational states, *Biochemistry 43*, 15204−15209.
42. Kihira, Y., Majima, E., Shinohara, Y., and Terada, H. (2005) Cysteine labeling studies detect conformational changes in region 106−132 of the mitochondrial ADP/ATP carrier of *Saccharomyces cerevisiae*, *Biochemistry 44*, 184−192.
43. Indiveri, C., Giangregorio, N., Iacobazzi, V., and Palmieri, F. (2002) Site-directed mutagenesis and chemical modification of the six native cysteine residues of the rat mitochondrial carnitine carrier: implications for the role of cysteine-136, *Biochemistry 41*, 8649−8656.
44. Yellen, G., Jurman, M. E., Abramson, T., and MacKinnon, R. (1991) Mutations affecting internal TEA blockade identify the probable pore-forming region of a K+ channel, *Science 251*, 939−942.
45. Kanner, B. I., and Borre, L. (2002) The dual-function glutamate transporters: structure and molecular characterisation of the substrate-binding sites, *Biochim. Biophys. Acta 1555*, 92−95.
46. Yernool, D., Boudker, O., Jin, Y., and Gouaux, E. (2004) Structure of a glutamate transporter homologue from *Pyrococcus horikoshii*, *Nature 431*, 811−818.
47. Doyle, D. A., Morais Cabral, J., Pfuetzner, R. A., Kuo, A., Gulbis, J. M., Cohen, S. L., Chait, B. T., and MacKinnon, R. (1998) The structure of the potassium channel: molecular basis of K+ conduction and selectivity, *Science 280*, 69−77.

BI0514820